PHYSICAL REVIEW D **96,** 035037 (2017)

Benchmarks for double Higgs production in the singlet-extended standard model at the LHC

Ian Lewis M. and Matthew Sullivan

Department of Physics and Astronomy, University of Kansas, Lawrence, Kansas 66045, USA
(Received 9 February 2017; published 31 August 2017)

The simplest extension of the standard model is to add a gauge singlet scalar, S: the singlet-extended standard model. In the absence of a Z_2 symmetry $S \to -S$ and if the new scalar is sufficiently heavy, this model can lead to resonant double Higgs production, significantly increasing the production rate over the standard model prediction. While searches for this signal are being performed, it is important to have benchmark points and models with which to compare the experimental results. In this paper we determine these benchmarks by maximizing the double Higgs production rate at the LHC in the singlet-extended standard model. We find that, within current constraints, the branching ratio of the new scalar into two standard model–like Higgs bosons can be upwards of 0.76, and the double Higgs rate can be increased upwards of 30 times the standard model prediction.

DOI: 10.1103/PhysRevD.96.035037

I. INTRODUCTION

One of the main objectives of the Large Hadron Collider (LHC) is to further our understanding of electroweak (EW) physics at the EW scale. Of particular interest are the interactions of the observed Higgs boson [1,2]. In fact, measurements of the Higgs production and decay rates are at the level of ∼20% precision [3]. Although these measurements help us determine if the observed Higgs boson is related to the source of fundamental masses within the standard model (SM), there are still many unanswered questions. One of the most pressing is the mechanism of EW symmetry breaking (EWSB). In the SM the source of EWSB is the scalar potential. Hence, it is interesting to study extensions of the SM that change the potential and their signatures at the LHC. In particular, simple extensions allow us to investigate phenomenology that is generic to more complete models.

The simplest extension of the SM is the addition of a gauge singlet real scalar, S: the singlet-extended SM. At the renormalizable level, the only allowed interactions between S and the SM are with the Higgs field. Hence, this model is a useful laboratory to investigate deviations from the SM Higgs potential. Although this is the simplest possible extension, it is well motivated. This scenario arises in Higgs portal models [4–13]. In these models, the scalar singlet couples to a dark matter sector. Through its interactions with the Higgs field, the new scalar provides couplings between the dark sector and the SM. Additionally, scalar singlets can help provide the strong first-order EW phase transition necessary for EW baryogenesis [13–30].

If there is no Z_2 symmetry, $S \to -S$, after EWSB the new scalar will mix with the SM Higgs boson. This mixing induces couplings between the new scalar and the rest of the SM particles. Hence, the new scalar can be produced and searched for at the LHC, as well as affecting precision Higgs measurements. The simplicity of the singlet-extended SM allows for easy interpretation of precision Higgs measurements [3,31] and resonant searches for heavy scalars [32–49].

There have been many phenomenological studies of the singlet-extended SM at the LHC [6,8,12,15,20,21,50–63]. Of particular interest to us is if the new scalar is sufficiently heavy, it can decay on shell into two SM-like Higgs bosons, mediating resonant double Higgs production at the LHC [19,64–75]. This can greatly enhance the double Higgs rate over the SM prediction. We will provide benchmark points that maximize double Higgs production in the singlet-extended SM. These benchmark points are needed to help determine when the experimental searches for resonant double Higgs production [35–41] are probing interesting regions of parameter space.[1]

In Sec. II we provide an overview of the model, including the theoretical constraints on the model. Experimental constraints are discussed in Sec. III. Resonant double Higgs production is discussed in Sec. IV. In Sec. V we discuss the maximization of the double Higgs rate and provide the benchmark points. We conclude with Sec. VI.

II. THE SINGLET-EXTENDED STANDARD MODEL

In this section we give an overview of the singlet-extended SM, following the notation of Ref. [66]. The results of Ref. [66] are important for establishing our benchmark points. Hence, we summarize the results of this paper regarding global minimization of the potential,

[1]A similar study has been done in the case of a broken Z_2 symmetry $S \to -S$ [70]. Here we work in the singlet-extended SM with no Z_2. This model has more free parameters allowing for different benchmark rates.

vacuum stability, and perturbative unitarity. In the remaining part of the paper we will extend upon this work, thoroughly investigating the relationship of these theoretical constraints and maximization of double Higgs production.

The model contains the SM Higgs doublet, H, and a new real gauge singlet scalar, S. The new singlet does not directly couple to SM particles except for the Higgs doublet. Allowing for all renormalizable terms, the most general scalar potential is

$$V(H,S) = -\mu^2 H^\dagger H + \lambda (H^\dagger H)^2 + \frac{a_1}{2} H^\dagger H S + \frac{a_2}{2} H^\dagger H S^2 + b_1 S + \frac{b_2}{2} S^2 + \frac{b_3}{3} S^3 + \frac{b_4}{4} S^4. \tag{1}$$

The neutral scalar component of H is denoted as $\phi_0 = (h+v)/\sqrt{2}$ with the vacuum expectation value (vev) being $\langle \phi_0 \rangle = \frac{v}{\sqrt{2}}$. We similarly write $S = s + x$, where the vev of S is denoted as x.

We require that EWSB occurs at an extremum of the potential, so that $v = v_{\mathrm{EW}} = 246$ GeV. Shifting the field $S \to S + \delta S$ does not introduce any new terms to the potential, and is only a meaningless change in parameters. Using this freedom, we can additionally choose that the EWSB minimum satisfies $x = 0$. Requiring that $(v,x) = (v_{\mathrm{EW}}, 0)$ be an extremum of the potential gives

$$\mu^2 = \lambda v_{\mathrm{EW}}^2, \qquad b_1 = -\frac{v_{\mathrm{EW}}^2}{4} a_1. \tag{2}$$

After symmetry breaking, there are two mass eigenstates denoted as h_1 and h_2 with masses m_1 and m_2, respectively. The new fields are related to the gauge eigenstate fields by

$$\begin{pmatrix} h_1 \\ h_2 \end{pmatrix} = \begin{pmatrix} \cos\theta & \sin\theta \\ -\sin\theta & \cos\theta \end{pmatrix} \begin{pmatrix} h \\ s \end{pmatrix}, \tag{3}$$

where θ is the mixing angle. The masses, m_1 and m_2, and the mixing angle, θ, are related to the scalar potential parameters

$$\begin{aligned} a_1 &= \frac{m_1^2 - m_2^2}{v_{\mathrm{EW}}} \sin 2\theta, \\ b_2 + \frac{a_2}{2} v_{\mathrm{EW}}^2 &= m_1^2 \sin^2\theta + m_2^2 \cos^2\theta, \\ \lambda &= \frac{m_1^2 \cos^2\theta + m_2^2 \sin^2\theta}{2 v_{\mathrm{EW}}^2}. \end{aligned} \tag{4}$$

We set the mass $m_1 = 125$ GeV to reproduce the discovered Higgs. The free parameter space is then

$$m_2, \theta, a_2, b_3, \quad \text{and} \quad b_4. \tag{5}$$

We are interested in the scenario with $m_2 \geq 2m_1$, where h_2 can decay on shell to two SM-like Higgs bosons, h_1. After symmetry breaking, the trilinear scalar terms in the potential which are relevant to double Higgs production are

$$V(h_1, h_2) \supset \frac{\lambda_{111}}{3!} h_1^3 + \frac{\lambda_{211}}{2!} h_2 h_1^2. \tag{6}$$

The trilinear coupling λ_{211} allows for the tree-level decay of $h_2 \to h_1 h_1$. At the EWSB minimum $(v,x) = (v_{\mathrm{EW}}, 0)$, the trilinear couplings are given by [66]

$$\begin{aligned} \lambda_{111} &= 2\sin^3\theta b_3 + \frac{3a_1}{2} \sin\theta \cos^2\theta + 3a_2 \sin^2\theta \cos\theta v_{\mathrm{EW}} + 6\lambda \cos^3\theta v_{\mathrm{EW}}, \\ \lambda_{211} &= 2\sin^2\theta \cos\theta b_3 + \frac{a_1}{2} \cos\theta (\cos^2\theta - 2\sin^2\theta) + (2\cos^2\theta - \sin^2\theta) \sin\theta v_{\mathrm{EW}} a_2 - 6\lambda \sin\theta \cos^2\theta v_{\mathrm{EW}}. \end{aligned} \tag{7}$$

A. Global minimization of the potential

The scalar potential, Eq. (1), allows for many extrema (v,x). There are two classes that need to be considered: $v \neq 0$ and $v = 0$. The $v \neq 0$ extrema are given by $(v,x) = (v_{\mathrm{EW}}, 0)$ and $(v,x) = (v_\pm, x_\pm)$ where [66]

$$\begin{aligned} x_\pm &\equiv \frac{v_{\mathrm{EW}}(3a_1 a_2 - 8b_3\lambda) \pm 8\sqrt{\Delta}}{4 v_{\mathrm{EW}}(4b_4\lambda - a_2^2)}, \\ v_\pm^2 &\equiv v_{\mathrm{EW}}^2 - \frac{1}{2\lambda}(a_1 x_\pm + a_2 x_\pm^2), \\ \Delta &= \frac{v_{\mathrm{EW}}^2}{64}(8b_3\lambda - 3a_1 a_2)^2 - \frac{m_1^2 m_2^2}{2}(4b_4\lambda - a_2^2). \end{aligned} \tag{8}$$

For all of these three solutions to be real, there are constraints $\Delta > 0$ and $v_\pm^2 > 0$.

The $v = 0$ extrema are given by solutions of the following cubic equation:

$$b_1 + b_2 x + b_3 x^2 + b_4 x^3 = 0. \tag{9}$$

Only real solutions for x are of interest. Manifestly real solutions for nondegenerate cubics are presented in the appendix.

As can be seen, there is only one extremum with $v = v_{\mathrm{EW}}$. Since the scalar S is a gauge singlet, it does not contribute to the gauge boson or SM fermion masses. Hence, to reproduce the correct EWSB pattern, we require that $(v_{\mathrm{EW}}, 0)$ is the global minimum.

B. Vacuum stability

To avoid instability of the vacuum from runaway negative energy solutions, the scalar potential should be bounded from below at large field values. Vacuum stability of the potential then requires that

$$4\lambda\phi_0^4 + 2a_2\phi_0^2 s^2 + b_4 s^2 > 0. \tag{10}$$

It is clear that bounding the potential from below along the axes $s = 0$ and $\phi_0 = 0$ requires

$$\lambda > 0 \quad \text{and} \quad b_4 > 0. \tag{11}$$

If $a_2 > 0$ as well, then the potential is always positive definite for large field values. However, $a_2 < 0$ is also allowed. Eq. (10) can be rewritten as

$$\lambda\left(2\phi_0^2 + \frac{a_2}{2\lambda}s^2\right)^2 + \left(b_4 - \frac{a_2^2}{4\lambda}\right)s^4 > 0. \tag{12}$$

The first term in Eq. (12) is always positive definite. Requiring the second term to be non-negative for $a_2 < 0$ gives the bound [66]

$$-2\sqrt{\lambda b_4} \leq a_2. \tag{13}$$

C. Perturbative unitarity

Perturbative unitarity of the partial wave expansion for the scattering also constrains quartic scalar couplings,

$$\mathcal{M} = 16\pi\sum_{j=0}^{\infty}(2j+1)a_j P_j(\cos\theta), \tag{14}$$

where $P_j(\cos\theta)$ are Legendre polynomials. Looking at the process $h_2h_2 \to h_2h_2$ for large energies, the first term in the partial wave expansion at leading order is

$$a_0(h_2h_2 \to h_2h_2) = \frac{3b_4}{8\pi}. \tag{15}$$

The perturbative unitarity requirement $|a_0| \leq 0.5$ gives the constraint $b_4 \lesssim 4.2$. When this bound is saturated, a minimum higher-order correction of 41% is needed to restore the unitarity of the amplitude [76].

There are also perturbative unitarity constraints on the other quartic couplings: $\lambda \lesssim 4.2$ and $a_2 \lesssim 25$. However, for all parameter points we consider, these constraints on λ and a_2 are automatically satisfied when all other constraints are applied.

III. EXPERIMENTAL CONSTRAINTS

The singlet model predicts that the couplings of h_1 to other SM fermions and gauge bosons are suppressed from the SM predictions by $\cos\theta$. Hence, the single Higgs production cross section is suppressed by $\cos^2\theta$,

$$\sigma(pp \to h_1) = \cos^2\theta\,\sigma_{\rm SM}(pp \to h_1), \tag{16}$$

where $\sigma_{\rm SM}(pp \to h_1)$ is the SM cross section for Higgs production at $m_1 = 125$ GeV. Since all couplings between h_1 and SM fermions and gauge bosons are universally suppressed, the branching ratios for h_1 decay agree with SM branching ratios,

$$\mathrm{BR}(h_1 \to X_{\rm SM}) = \mathrm{BR}_{\rm SM}(h_1 \to X_{\rm SM}), \tag{17}$$

where $X_{\rm SM}$ is any allowed SM final state. Using these properties, the most stringent constraint from observed Higgs signal strengths is from ATLAS: $\sin^2\theta \leq 0.12$ at 95% C.L. [31].

As mentioned earlier, there are also direct constraints from searches for heavy scalar particles [32–49]. For the mass range 250 GeV $\leq m_2 \leq$ 1000 GeV considered here, the direct constraints on $\sin\theta$ are weaker than those from the Higgs signal strengths [70]. Nevertheless, independently and using HiggsBounds [77–81], we verify that our benchmark points satisfy all experimental constraints.

IV. PRODUCTION AND DECAY RATES

The contributions to double Higgs production in the singlet model are shown in Fig. 1. Figures 1(a) and 1(b) are present in the SM double Higgs production, while the s-channel h_2 contribution in Fig. 1(c) is responsible for the resonant h_1h_1 production. The s-channel h_1 (h_2) contribution in Fig. 1(b) [Fig. 1(c)] depends on the scalar trilinear couplings λ_{111} (λ_{211}) in Eq. (7). Hence, this process is clearly sensitive to the shape of the scalar potential.

It is expected that the resonant h_2 contribution dominates the double Higgs production cross section. We then use the narrow width approximation as follows:

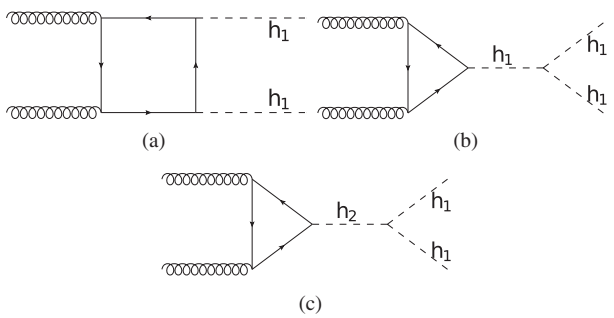

FIG. 1. Representative diagrams for double Higgs production corresponding to (a) box diagram, (b) triangle diagram with the s-channel SM-like Higgs boson h_1, and (c) triangle diagram with the resonant s-channel h_2. The top quark loops are the dominant contribution to the production.

$$\sigma(pp \to h_2 \to h_1 h_1) \approx \sigma(pp \to h_2)\mathrm{BR}(h_2 \to h_1 h_1). \quad (18)$$

Although interference effects between the different contributions in Fig. 1 can be significant [68], our purpose here is to maximize the double Higgs rate in this model. Hence, for simplicity we focus on maximizing the cross section in Eq. (18). This is sufficient to attain our goal.

Due to mixing with the Higgs boson, h_2 has couplings to SM fermions and gauge bosons proportional to $\sin\theta$. The cross section for production of h_2 is then

$$\sigma(pp \to h_2) = \sin^2\theta \sigma_{\mathrm{SM}}(pp \to h_2) \quad (19)$$

with $\sigma_{\mathrm{SM}}(pp \to h_2)$ being the SM Higgs production cross section evaluated at a Higgs mass of m_2. Since the couplings to fermions and gauge bosons are proportional to the SM values, the intuition about the dominant SM Higgs production channels is valid for the production of h_2. Hence, gluon fusion $gg \to h_2$ is the dominant channel, as illustrated in Fig. 1(c).

The heavy scalar h_2 can decay to SM gauge bosons and fermions with partial widths of

$$\Gamma(h_2 \to X_{\mathrm{SM}}) = \sin^2\theta \Gamma_{\mathrm{SM}}(h_2 \to X_{\mathrm{SM}}), \quad (20)$$

where $\Gamma_{\mathrm{SM}}(h_2 \to X_{\mathrm{SM}})$ is the SM decay width for a Higgs boson into SM final states $X_{\mathrm{SM}} \neq h_1 h_1$ evaluated at a mass of m_2. The tree-level decay for $h_2 \to h_1 h_1$ has a partial width given by

$$\Gamma(h_2 \to h_1 h_1) = \frac{\lambda_{211}^2}{32\pi m_2}\sqrt{1 - \frac{4m_1^2}{m_2^2}}. \quad (21)$$

The branching ratio for $h_2 \to h_1 h_1$ is

$$\mathrm{BR}(h_2 \to h_1 h_1) = \frac{\Gamma(h_2 \to h_1 h_1)}{\Gamma(h_2)}, \quad (22)$$

where

$$\Gamma(h_2) = \Gamma(h_2 \to h_1 h_1) + \sin^2\theta \Gamma_{\mathrm{SM}}(h_2 \to X_{\mathrm{SM}}) \quad (23)$$

is the total width of h_2.

The parameter b_4 does not explicitly affect $\mathrm{BR}(h_2 \to h_1 h_1)$. However, through the constraints of vacuum stability and $(v, x) = (v_{\mathrm{EW}}, 0)$ being the global minimum of the scalar potential (Sec. II A), b_4 affects the allowed ranges for the other parameters a_2 and b_3. These parameters appear in the trilinear coupling λ_{211} in Eq. (7), which is relevant for $\Gamma(h_2 \to h_1 h_1)$. Figure 2 shows the allowed parameter region satisfying these constraints for (a) $b_4 = 4.2$ and (b) $b_4 = 0.2$ with $m_2 = 260$ GeV and $\sin^2\theta = 0.12$. It is clear from the figures that a lower value of b_4 shrinks the allowed region. The shading in the figures indicates the value of $\mathrm{BR}(h_2 \to h_1 h_1)$, where the values of

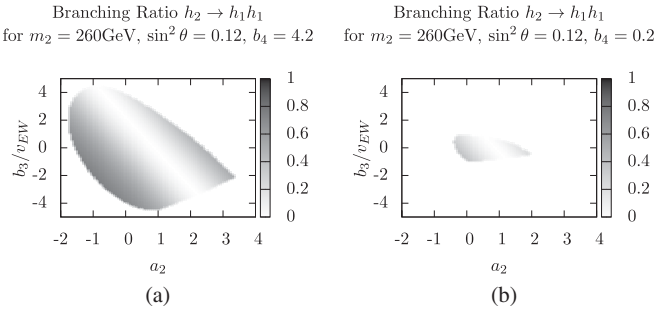

FIG. 2. $\mathrm{BR}(h_2 \to h_1 h_1)$ as a function of b_3 and a_2 for $m_2 = 260$ GeV and $\sin^2\theta = 0.12$. In (a) $b_4 = 4.2$ and (b) $b_4 = 0.2$. The shaded regions are allowed by the global minimum constraint. The darker shaded regions have larger $\mathrm{BR}(h_2 \to h_1 h_1)$.

$\Gamma_{\mathrm{SM}}(h_2 \to X_{\mathrm{SM}})$ were obtained from Ref. [82]. It was found that the maximum $\mathrm{BR}(h_2 \to h_1 h_1)$ always occurs with $b_4 = 4.2$ at the unitarity bound.

In Fig. 3 we show allowed ranges of $\Gamma(h_2)/m_2$ as a function of the mass of m_2 for $b_4 = 4.2$ and $\sin^2\theta = 0.12$. The total width is always bounded by $\Gamma(h_2)/m_2 \lesssim 0.09$. For $m_2 \lesssim 700$ GeV, we also have $\Gamma(h_2)/m_2 \lesssim 0.05$. As $\sin\theta$ decreases below its upper bound, the total width of h_2 will decrease as well. The value of b_4 has no effect on the partial widths of h_2 into SM fermions or gauge bosons. However, as b_4 decreases, the partial width of $\Gamma(h_2 \to h_1 h_1)$ decreases as shown in Fig. 2. Hence, the upper bound on $\Gamma(h_2)$ in Fig. 3 is the upper bound throughout the allowed parameter regions, and h_2 is sufficiently narrow to justify the narrow width approximation in Eq. (18).

V. RESULTS

We maximize the production rate in Eq. (18) by fixing m_2 and θ, then scanning over the remaining parameters

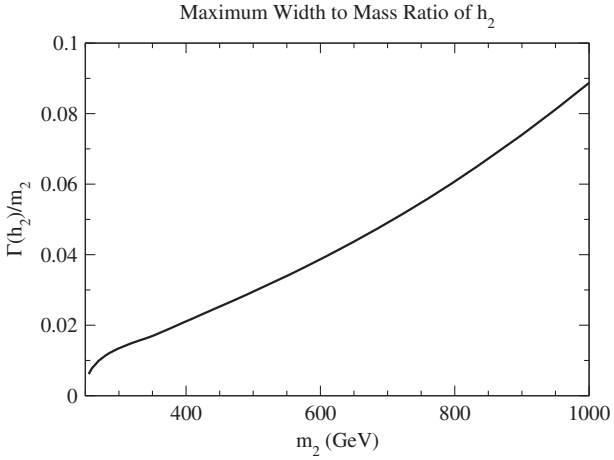

FIG. 3. The ranges of $\Gamma(h_2)/m_2$ allowed by the theoretical constraints in Secs. II A and II B as a function of m_2 for $b_4 = 4.2$ and $\sin^2\theta = 0.12$.

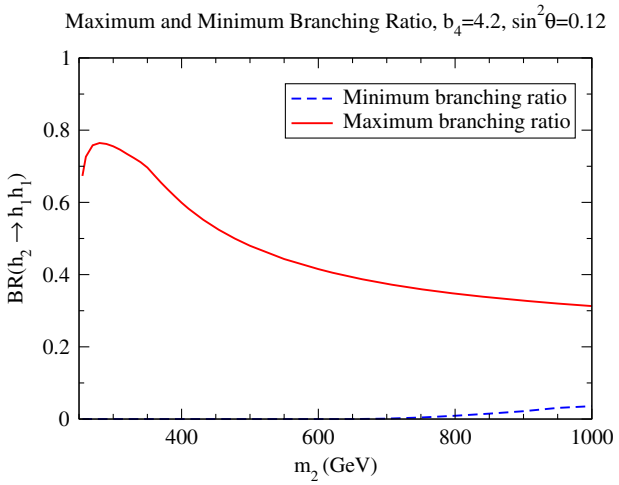

FIG. 4. Maximum and minimum allowed $\mathrm{BR}(h_2 \to h_1 h_1)$ as a function of m_2 for $b_4 = 4.2$ and $\sin^2\theta = 0.12$.

$$a_2, b_3, \quad \text{and} \quad b_4. \tag{24}$$

For all numerical results, the SM production cross sections and widths for a Higgs boson in Eqs. (16), (17), (19), and (20) were obtained from Ref. [82].

The maximum and minimum $\mathrm{BR}(h_2 \to h_1 h_1)$ for different values of m_2 are shown in Fig. 4. We set $b_4 = 4.2$ at the perturbative unitarity bound and $\sin^2\theta = 0.12$ at the experimental bound [31]. The largest possible branching ratio occurs at around 280 GeV with $\mathrm{BR}(h_2 \to h_1 h_1) = 0.76$. Even up to masses of 1000 GeV the branching ratio to double Higgs can be larger than 0.3. Additionally, for $m_2 \gtrsim 600$ GeV there is a minimum on $\mathrm{BR}(h_2 \to h_1 h_1)$.

Figure 5(a) shows the dependence of the maximum branching ratio $\mathrm{BR}(h_2 \to h_1 h_1)$ on the parameter b_4. As can be seen, if the parameter b_4 is less than the unitarity bound of 4.2, then the largest possible branching ratio becomes smaller. This is due to the shrinking of the allowed range for the parameters a_2 and b_3, as shown in Fig. 2. Even for small values of b_4, the branching ratio can still be quite substantial.

The maximum possible value of $\sin^2\theta$ is expected to decrease as more data is taken at the LHC and the measurements of the observed Higgs couplings become more precise. Figure 5(b) shows the maximum possible $\mathrm{BR}(h_2 \to h_1 h_1)$ for several values of $\sin^2\theta$. As can be seen, the branching ratio can be larger for smaller $\sin\theta$. Hence, maximization of $\mathrm{BR}(h_2 \to h_1 h_1)$ occurs at small $\sin\theta$. However, double Higgs production is not maximized with this condition.

Now we turn our attention to maximizing the double Higgs production rate. Figure 6 shows the maximum $\sigma(pp \to h_2)\mathrm{BR}(h_2 \to h_1 h_1)$ at an LHC energy of $\sqrt{S_H} = 13$ TeV for various (a) b_4 and (b) $\sin\theta$ values as a function of mass m_2. The values are scaled by the SM double Higgs production cross section at 13 TeV of $33.53^{+5.3\%}_{-6.8\%}$ fb [82], calculated at next-to-next-to-leading log matched to next-to-next-to-leading order in QCD with next-to-leading order top quark mass dependence [83]. As mentioned earlier, the maximum rates occur when b_4 is at the unitarity bound $b_4 = 4.2$. For $\sin\theta$, although the maximum $\mathrm{BR}(h_2 \to h_1 h_1)$ increases as $\sin\theta$ decreases, this increase is not enough to compensate for the $\sin^2\theta$ suppression of the production cross section $\sigma(pp \to h_2)$ in Eq. (19). Hence, the maximum double Higgs production cross section occurs at the experimental bound $\sin^2\theta = 0.12$. In the best case, the resonant double Higgs production is roughly 30 times the SM double Higgs cross section.

Finally, we provide our benchmark points in Tables I and II. We provide the parameter points that maximize the $h_1 h_1$ production in the singlet-extended SM, as well as the corresponding $\mathrm{BR}(h_2 \to h_1 h_1)$ and $h_1 h_1$ production cross

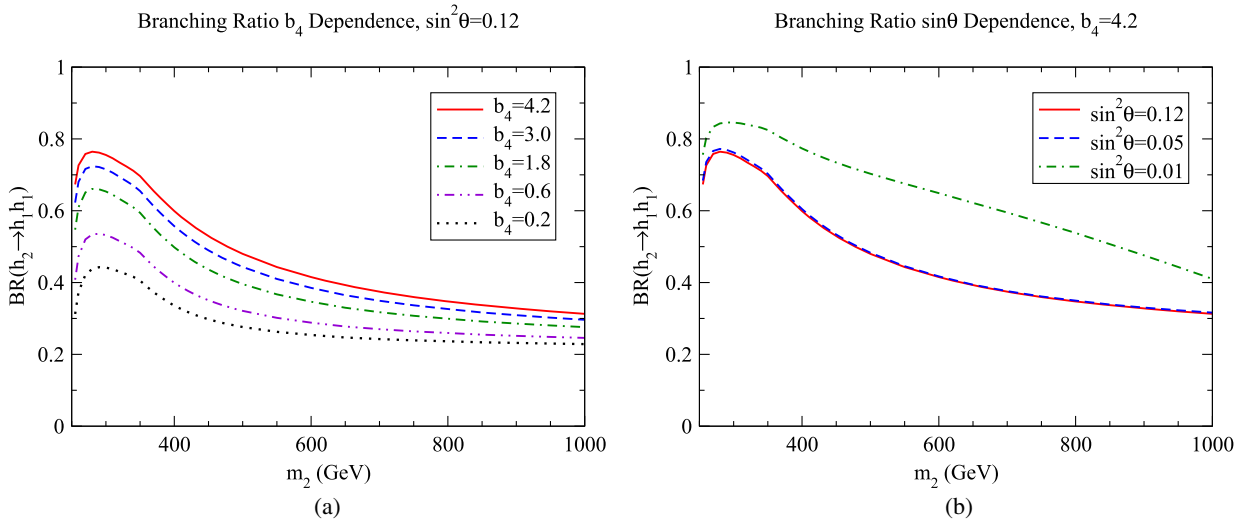

FIG. 5. Maximum allowed $\mathrm{BR}(h_2 \to h_1 h_1)$ as a function of m_2 for different values of (a) b_4 and (b) $\sin\theta$.

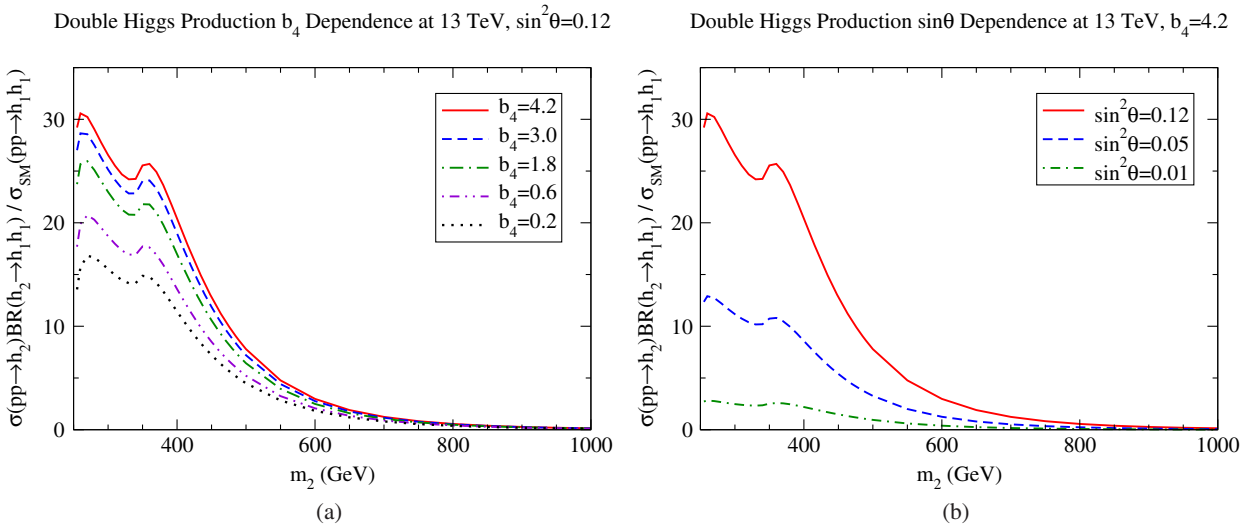

FIG. 6. Maximum $\sigma(pp \to h_2)\mathrm{BR}(h_2 \to h_1 h_1)$, scaled by the calculated SM double Higgs production, as a function of m_2 for different values of (a) b_4 and (b) $\sin\theta$.

section at a lab frame energy of $\sqrt{S_H} = 13$ TeV. As discussed before, the maximum $\mathrm{BR}(h_2 \to h_1 h_1)$ occurs for $b_4 = 4.2$ at the unitarity bound. Hence, we fix $b_4 = 4.2$ for all benchmark points. Also, the maximum $h_1 h_1$ production cross section occurs for $\sin^2\theta = 0.12$ at the current limit [31]. Table I contains the benchmark points for $\sin^2\theta = 0.12$. However, as mentioned earlier, as the LHC continues to gather data it is expected that the precision Higgs measurements will further limit $\sin\theta$. The uncertainties in Higgs coupling measurements are projected to be ~5% with 3000 fb^{-1} of integrated luminosity at the LHC [84]. This corresponds to a bound of $\sin^2\theta \lesssim 0.05$ due to the overall $\cos^2\theta$ suppression of the h_1 rate of production. Hence, we also provide benchmark points for $\sin^2\theta = 0.05$ in Table II.

TABLE I. Benchmark points that maximize $\mathrm{BR}(h_2 \to h_1 h_1)$ with $b_4 = 4.2$ and $\sin^2\theta = 0.12$. The cross sections are evaluated at a lab frame energy of $\sqrt{S_H} = 13$ TeV.

m_2	a_2	b_3/v_{EW}	$\mathrm{BR}(h_2 \to h_1 h_2)$	$\sigma(pp \to h_2)\times \mathrm{BR}(h_2 \to h_1 h_1)$
300 GeV	−0.79	−2.7	0.76	0.89 pb
400 GeV	−0.40	−3.9	0.60	0.68 pb
500 GeV	0.059	−5.4	0.48	0.26 pb
600 GeV	0.56	−7.1	0.42	0.10 pb
700 GeV	1.0	−8.7	0.37	0.042 pb
800 GeV	1.6	−11	0.35	0.019 pb

TABLE II. Benchmark points that maximize $\mathrm{BR}(h_2 \to h_1 h_1)$ with $b_4 = 4.2$ and $\sin^2\theta = 0.05$. The cross sections are evaluated at a lab frame energy of $\sqrt{S_H} = 13$ TeV.

m_2	a_2	b_3/v_{EW}	$\mathrm{BR}(h_2 \to h_1 h_2)$	$\sigma(pp \to h_2)\times \mathrm{BR}(h_2 \to h_1 h_1)$
300 GeV	−1.2	−1.6	0.76	0.37 pb
400 GeV	−1.0	−2.7	0.60	0.29 pb
500 GeV	−0.78	−3.9	0.48	0.11 pb
600 GeV	−0.59	−5.0	0.42	0.042 pb
700 GeV	−0.31	−6.5	0.38	0.017 pb
800 GeV	−0.015	−8.1	0.35	0.0079 pb

VI. CONCLUSION

The simplest possible extension of the SM is the addition of a real gauge singlet scalar. Although simple, this model is theoretically well motivated and has interesting phenomenology. In particular, if the new scalar h_2 is sufficiently heavy $m_2 \geq 2m_1$, this model can give rise to resonant double Higgs production at the LHC. We have investigated this signature. We determined benchmark parameter points that maximize the double Higgs production rate in this model at the $\sqrt{S_H} = 13$ TeV LHC. These benchmark points are important for gauging when the ongoing experimental searches for resonant double Higgs production are probing interesting regions of parameter space of well-motivated models. We have found that $\mathrm{BR}(h_2 \to h_1 h_1)$ as high as 0.76 and $h_1 h_1$ production rates up to 30 times the SM rate are still possible.

ACKNOWLEDGMENTS

We thank S. Dawson for valuable discussions about double Higgs production in the singlet-extended SM. This investigation was supported in part by the University of Kansas General Research Fund allocation 2302091.

APPENDIX: $v = 0$ EXTREMA

In this appendix we give solutions to Eq. (9) where $v = 0$. We update the results from Ref. [66], presenting these solutions in a manifestly real form.

Solutions to the extrema conditions were solutions to Eq. (9), repeated below.

$$b_1 + b_2 x + b_3 x^2 + b_4 x^3 = 0 \tag{A1}$$

All the coefficients in Eq. (A1) are real. We divide Eq. (A1) by b_4 to normalize the cubic term,

$$\begin{aligned} x^3 + Ax^2 + Bx + C &= 0 \\ A &= \frac{b_3}{b_4} \\ B &= \frac{b_2}{b_4} \\ C &= \frac{b_1}{b_4} \end{aligned} \tag{A2}$$

We define the intermediate variables Q and R as

$$Q = \frac{3B - A^2}{9}, \tag{A3}$$

$$R = \frac{9AB - 27C - 2A^3}{54}. \tag{A4}$$

The polynomial discriminant of Eq. (A2) is then given by

$$D = Q^3 + R^2. \tag{A5}$$

The discriminant D can be either positive, negative, or zero. If the discriminant is zero, the cubic has degenerate solutions. The parameter space where $D = 0$ has zero volume, so it is unlikely to occur. The degenerate solutions are not important to consider for our purposes. If $D < 0$, the cubic has three distinct real roots. If $D > 0$, the cubic has a real root and a pair of complex conjugate roots.

For the case $D < 0$, we define an angle θ as follows:

$$\theta = \cos^{-1}\left(\frac{R}{-Q}\sqrt{\frac{1}{-Q}}\right). \tag{A6}$$

Note that if $D < 0$, then we also must have $Q < 0$. The three real solutions to Eq. (A1) are then given by

$$\begin{aligned} x_1 &= 2\sqrt{-Q}\cos\left(\frac{\theta}{3}\right) - \frac{A}{3}, \\ x_2 &= 2\sqrt{-Q}\cos\left(\frac{\theta + 2\pi}{3}\right) - \frac{A}{3}, \\ x_3 &= 2\sqrt{-Q}\cos\left(\frac{\theta + 4\pi}{3}\right) - \frac{A}{3}. \end{aligned} \tag{A7}$$

For the case $D > 0$, we must look at two subcases. If $Q < 0$, we then define a hyperbolic angle η as follows:

$$\eta = \cosh^{-1}\left(\frac{|R|}{Q}\sqrt{\frac{1}{-Q}}\right). \tag{A8}$$

The single real solution to Eq. (A1) is then given by

$$x = 2\frac{|R|}{R}\sqrt{-Q}\cosh\left(\frac{\eta}{3}\right) - \frac{A}{3}. \tag{A9}$$

For the case $D > 0$ and $Q > 0$, we also define a hyperbolic angle η as follows:

$$\eta = \sinh^{-1}\left(\frac{R}{Q}\sqrt{\frac{1}{Q}}\right). \tag{A10}$$

The single real solution to Eq. (A1) is then given by

$$x = 2\sqrt{Q}\sinh\left(\frac{\eta}{3}\right) - \frac{A}{3}. \tag{A11}$$

[1] S. Chatrchyan *et al.* (CMS Collaboration), Observation of a new boson at a mass of 125 GeV with the CMS experiment at the LHC, Phys. Lett. B **716**, 30 (2012).

[2] G. Aad *et al.* (ATLAS Collaboration), Observation of a new particle in the search for the Standard Model Higgs boson with the ATLAS detector at the LHC, Phys. Lett. B **716**, 1 (2012).

[3] G. Aad *et al.* (ATLAS and CMS Collaborations), Measurements of the Higgs boson production and decay rates and constraints on its couplings from a combined ATLAS and CMS analysis of the LHC pp collision data at $\sqrt{s} = 7$ and 8 TeV, J. High Energy Phys. 08 (2016) 045.

[4] T. Binoth and J. J. van der Bij, Influence of strongly coupled hidden scalars on Higgs signals, Z. Phys. C **75**, 17 (1997).

[5] H. Davoudiasl, R. Kitano, T. Li, and H. Murayama, The new minimal standard model, Phys. Lett. B **609**, 117 (2005).

[6] R. M. Schabinger and J. D. Wells, Minimal spontaneously broken hidden sector and its impact on Higgs boson physics at the large hadron collider, Phys. Rev. D **72**, 093007 (2005).

[7] B. Patt and F. Wilczek, Higgs-field portal into hidden sectors, arXiv:hep-ph/0605188.
[8] M. Bowen, Y. Cui, and J. D. Wells, Narrow trans-TeV Higgs bosons and $H \to hh$ decays: Two LHC search paths for a hidden sector Higgs boson, J. High Energy Phys. 03 (2007) 036.
[9] S. Bock, R. Lafaye, T. Plehn, M. Rauch, D. Zerwas, and P. M. Zerwas, Measuring hidden Higgs and strongly interacting Higgs scenarios, Phys. Lett. B **694**, 44 (2010).
[10] A. Djouadi, O. Lebedev, Y. Mambrini, and J. Quevillon, Implications of LHC searches for Higgs-portal dark matter, Phys. Lett. B **709**, 65 (2012).
[11] C. Englert, T. Plehn, M. Rauch, D. Zerwas, and P. M. Zerwas, LHC: Standard Higgs and hidden Higgs, Phys. Lett. B **707**, 512 (2012).
[12] C. Englert, T. Plehn, D. Zerwas, and P. M. Zerwas, Exploring the Higgs portal, Phys. Lett. B **703**, 298 (2011).
[13] T. Alanne, K. Tuominen, and V. Vaskonen, Strong phase transition, dark matter and vacuum stability from simple hidden sectors, Nucl. Phys. **B889**, 692 (2014).
[14] S. W. Ham, Y. S. Jeong, and S. K. Oh, Electroweak phase transition in an extension of the standard model with a real Higgs singlet, J. Phys. G **31**, 857 (2005).
[15] S. Profumo, M. J. Ramsey-Musolf, and G. Shaughnessy, Singlet Higgs phenomenology and the electroweak phase transition, J. High Energy Phys. 08 (2007) 010.
[16] A. Ashoorioon and T. Konstandin, Strong electroweak phase transitions without collider traces, J. High Energy Phys. 07 (2009) 086.
[17] D. Bodeker and G. D. Moore, Can electroweak bubble walls run away?, J. Cosmol. Astropart. Phys. 05 (2009) 009.
[18] J. R. Espinosa, T. Konstandin, and F. Riva, Strong electroweak phase transitions in the Standard Model with a singlet, Nucl. Phys. **B854**, 592 (2012).
[19] J. M. No and M. Ramsey-Musolf, Probing the Higgs portal at the LHC through resonant di-Higgs production, Phys. Rev. D **89**, 095031 (2014).
[20] D. Curtin, P. Meade, and C.-T. Yu, Testing electroweak baryogenesis with future colliders, J. High Energy Phys. 11 (2014) 127.
[21] S. Profumo, M. J. Ramsey-Musolf, C. L. Wainwright, and P. Winslow, Singlet-catalyzed electroweak phase transitions and precision Higgs boson studies, Phys. Rev. D **91**, 035018 (2015).
[22] F. P. Huang and C. S. Li, Electroweak baryogenesis in the framework of the effective field theory, Phys. Rev. D **92**, 075014 (2015).
[23] P. H. Damgaard, A. Haarr, D. O'Connell, and A. Tranberg, Effective field theory and electroweak baryogenesis in the singlet-extended Standard Model, J. High Energy Phys. 02 (2016) 107.
[24] J. Kozaczuk, Bubble expansion and the viability of singlet-driven electroweak baryogenesis, J. High Energy Phys. 10 (2015) 135.
[25] P. Huang, A. Joglekar, B. Li, and C. E. M. Wagner, Probing the electroweak phase transition at the LHC, Phys. Rev. D **93**, 055049 (2016).
[26] M.-L. Xiao and J.-H. Yu, Electroweak baryogenesis in a scalar-assisted vectorlike fermion model, Phys. Rev. D **94**, 015011 (2016).
[27] P. Huang, A. J. Long, and L.-T. Wang, Probing the electroweak phase transition with Higgs factories and gravitational waves, Phys. Rev. D **94**, 075008 (2016).
[28] A. V. Kotwal, M. J. Ramsey-Musolf, J. M. No, and P. Winslow, Singlet-catalyzed electroweak phase transitions in the 100 TeV frontier, Phys. Rev. D **94**, 035022 (2016).
[29] D. Curtin, P. Meade, and H. Ramani, Thermal resummation and phase transitions, arXiv:1612.00466.
[30] V. Vaskonen, Electroweak baryogenesis and gravitational waves from a real scalar singlet, Phys. Rev. D **95**, 123515 (2017).
[31] G. Aad *et al.* (ATLAS Collaboration), Constraints on new phenomena via Higgs boson couplings and invisible decays with the ATLAS detector, J. High Energy Phys. 11 (2015) 206.
[32] G. Aad *et al.* (ATLAS Collaboration), Search for a high-mass Higgs boson decaying to a W boson pair in pp collisions at $\sqrt{s} = 8$ TeV with the ATLAS detector, J. High Energy Phys. 01 (2016) 032.
[33] V. Khachatryan *et al.* (CMS Collaboration), Search for a Higgs boson in the mass range from 145 to 1000 GeV decaying to a pair of W or Z bosons, J. High Energy Phys. 10 (2015) 144.
[34] G. Aad *et al.* (ATLAS Collaboration), Search for an additional heavy Higgs boson in the $H \to ZZ$ decay channel at $\sqrt{s} = 8$ TeV in pp collision data with the ATLAS detector, Eur. Phys. J. C **76**, 45 (2016).
[35] G. Aad *et al.* (ATLAS Collaboration), Searches for Higgs boson pair production in the $hh \to bb\tau\tau$, $\gamma\gamma WW^*$, $\gamma\gamma bb$, $bbbb$ channels with the ATLAS detector, Phys. Rev. D **92**, 092004 (2015).
[36] V. Khachatryan *et al.* (CMS Collaboration), Search for resonant pair production of Higgs bosons decaying to two bottom quark-antiquark pairs in proton-proton collisions at 8 TeV, Phys. Lett. B **749**, 560 (2015).
[37] V. Khachatryan *et al.* (CMS Collaboration), Search for two Higgs bosons in final states containing two photons and two bottom quarks in proton-proton collisions at 8 TeV, Phys. Rev. D **94**, 052012 (2016).
[38] CMS Collaboration, Report No. CMS-PAS-HIG-16-029.
[39] CMS Collaboration, Report No. CMS-PAS-HIG-16-002.
[40] ATLAS Collaboration, Report No. ATLAS-CONF-2016-049.
[41] ATLAS Collaboration, Report No. ATLAS-CONF-2016-004.
[42] CMS Collaboration, Report No. CMS-PAS-HIG-16-033.
[43] CMS Collaboration, Report No. CMS-PAS-HIG-16-023.
[44] ATLAS Collaboration, Report No. ATLAS-CONF-2016-079.
[45] ATLAS Collaboration, Report No. ATLAS-CONF-2016-074.
[46] M. Aaboud *et al.* (ATLAS Collaboration), Searches for heavy diboson resonances in pp collisions at $\sqrt{s} = 13$ TeV with the ATLAS detector, J. High Energy Phys. 09 (2016) 173.
[47] CMS Collaboration, Report No. CMS-PAS-B2G-15-002.
[48] V. Khachatryan *et al.* (CMS Collaboration), Search for resonant $t\bar{t}$ production in proton-proton collisions at $\sqrt{s} = 8$ TeV, Phys. Rev. D **93**, 012001 (2016).

[49] G. Aad *et al.* (ATLAS Collaboration), A search for $t\bar{t}$ resonances using lepton-plus-jets events in proton-proton collisions at $\sqrt{s} = 8$ TeV with the ATLAS detector, J. High Energy Phys. 08 (2015) 148.
[50] D. O'Connell, M. J. Ramsey-Musolf, and M. B. Wise, Minimal extension of the Standard Model scalar sector, Phys. Rev. D **75**, 037701 (2007).
[51] V. Barger, P. Langacker, M. McCaskey, M. Ramsey-Musolf, and G. Shaughnessy, Complex singlet extension of the Standard Model, Phys. Rev. D **79**, 015018 (2009).
[52] S. Dawson and W. Yan, Hiding the Higgs boson with multiple scalars, Phys. Rev. D **79**, 095002 (2009).
[53] D. Bertolini and M. McCullough, The social Higgs, J. High Energy Phys. 12 (2012) 118.
[54] G. M. Pruna and T. Robens, Higgs singlet extension parameter space in the light of the LHC discovery, Phys. Rev. D **88**, 115012 (2013).
[55] C. Caillol, B. Clerbaux, J.-M. Frère, and S. Mollet, Precision versus discovery: A simple benchmark, Eur. Phys. J. Plus **129**, 93 (2014).
[56] D. López-Val and T. Robens, Δr and the W-boson mass in the singlet extension of the standard model, Phys. Rev. D **90**, 114018 (2014).
[57] D. Buttazzo, F. Sala, and A. Tesi, Singlet-like Higgs bosons at present and future colliders, J. High Energy Phys. 11 (2015) 158.
[58] T. Robens and T. Stefaniak, Status of the Higgs singlet extension of the Standard Model after LHC run 1, Eur. Phys. J. C **75**, 104 (2015).
[59] A. Falkowski, C. Gross, and O. Lebedev, A second Higgs from the Higgs portal, J. High Energy Phys. 05 (2015) 057.
[60] F. Bojarski, G. Chalons, D. Lopez-Val, and T. Robens, Heavy to light Higgs boson decays at NLO in the singlet extension of the Standard Model, J. High Energy Phys. 02 (2016) 147.
[61] R. Costa, M. Mühlleitner, M. O. P. Sampaio, and R. Santos, Singlet extensions of the Standard Model at LHC run 2: Benchmarks and comparison with the NMSSM, J. High Energy Phys. 06 (2016) 034.
[62] O. Fischer, Clues on the Majorana scale from scalar resonances at the LHC, Mod. Phys. Lett. A **32**, 1750035 (2017).
[63] S. Fichet, G. von Gersdorff, E. Pontón, and R. Rosenfeld, The global Higgs as a signal for compositeness at the LHC, J. High Energy Phys. 01 (2017) 012.
[64] M. J. Dolan, C. Englert, and M. Spannowsky, New Physics in LHC Higgs boson pair production, Phys. Rev. D **87**, 055002 (2013).
[65] B. Cooper, N. Konstantinidis, L. Lambourne, and D. Wardrope, Boosted $hh \to b\bar{b}b\bar{b}$: A new topology in searches for TeV-scale resonances at the LHC, Phys. Rev. D **88**, 114005 (2013).
[66] C.-Y. Chen, S. Dawson, and I. M. Lewis, Exploring resonant di-Higgs boson production in the Higgs singlet model, Phys. Rev. D **91**, 035015 (2015).
[67] V. Martn Lozano, J. M. Moreno, and C. B. Park, Resonant Higgs boson pair production in the $hh \to b\bar{b}WW \to b\bar{b}\ell^+\nu\ell^-\bar{\nu}$ decay channel, J. High Energy Phys. 08 (2015) 004.
[68] S. Dawson and I. M. Lewis, NLO corrections to double Higgs boson production in the Higgs singlet model, Phys. Rev. D **92**, 094023 (2015).
[69] S. I. Godunov, A. N. Rozanov, M. I. Vysotsky, and E. V. Zhemchugov, Extending the Higgs sector: An extra singlet, Eur. Phys. J. C **76**, 1 (2016).
[70] T. Robens and T. Stefaniak, LHC benchmark scenarios for the real Higgs singlet extension of the Standard Model, Eur. Phys. J. C **76**, 268 (2016).
[71] K. Nakamura, K. Nishiwaki, K.-y. Oda, S. C. Park, and Y. Yamamoto, Di-higgs enhancement by neutral scalar as probe of new colored sector, Eur. Phys. J. C **77**, 273 (2017).
[72] T. Huang, J. M. No, L. Pernié, M. Ramsey-Musolf, A. Safonov, M. Spannowsky, and P. Winslow, Resonant di-Higgs production in the $b\bar{b}WW$ channel: Probing the electroweak phase transition at the LHC, arXiv:1701.04442.
[73] J. Chang, C.-R. Chen, and C.-W. Chiang, Higgs boson pair productions in the Georgi-Machacek model at the LHC, J. High Energy Phys. 03 (2017) 137.
[74] L.-C. Lü, C. Du, Y. Fang, H.-J. He, and H. Zhang, Searching for heavier Higgs boson via di-Higgs production at LHC run 2, Phys. Lett. B **755**, 509 (2016).
[75] J. Ren, R.-Q. Xiao, M. Zhou, Y. Fang, H.-J. He, and W. Yao, LHC search of new Higgs boson via resonant di-Higgs production with decays into 4 W, arXiv:1706.05980.
[76] A. Schuessler and D. Zeppenfeld, Unitarity constraints on MSSM trilinear couplings, in *SUSY 2007 Proceedings, 15th International Conference on Supersymmetry and Unification of Fundamental Interactions, July 26–August 1, 2007, Karlsruhe, Germany*, p. 236, http://arxiv.org/pdf/0710.5175.pdf.
[77] P. Bechtle, O. Brein, S. Heinemeyer, G. Weiglein, and K. E. Williams, HiggsBounds: Confronting arbitrary Higgs sectors with exclpusion bounds from LEP and the Tevatron, Comput. Phys. Commun. **181**, 138 (2010).
[78] P. Bechtle, O. Brein, S. Heinemeyer, G. Weiglein, and K. E. Williams, HiggsBounds 2.0.0: Confronting neutral and charged Higgs sector predictions with exclusion bounds from LEP and the Tevatron, Comput. Phys. Commun. **182**, 2605 (2011).
[79] P. Bechtle *et al.*, *Proc. Sci.*, CHARGED2012 (2012) 024, [arXiv:1301.2345].
[80] P. Bechtle, O. Brein, S. Heinemeyer, O. Stål, T. Stefaniak, G. Weiglein, and K. E. Williams, HiggsBounds-4: Improved tests of extended Higgs sectors against exclusion bounds from LEP, the Tevatron and the LHC, Eur. Phys. J. C **74**, 2693 (2014).
[81] P. Bechtle, S. Heinemeyer, O. Stal, T. Stefaniak, and G. Weiglein, Applying exclusion likelihoods from LHC searches to extended Higgs sectors, Eur. Phys. J. C **75**, 421 (2015).
[82] D. de Florian *et al.* (LHC Higgs Cross Section Working Group Collaboration), Handbook of LHC Higgs cross sections: 4. Deciphering the nature of the Higgs sector, arXiv:1610.07922.
[83] S. Borowka, N. Greiner, G. Heinrich, S. P. Jones, M. Kerner, J. Schlenk, and T. Zirke, Full top quark mass dependence in Higgs boson pair production at NLO, J. High Energy Phys. 10 (2016) 107.
[84] S. Dawson *et al.*, Working Group Report: Higgs Boson, in *Proceedings, 2013 Community Summer Study on the Future of U.S. Particle Physics: Snowmass on the Mississippi (CSS2013): Minneapolis, MN, USA, July 29–August 6, 2013*, http://inspirehep.net/record/1262795/files/arXiv:1310.8361.pdf.